Morphology, structure, and growth of nanoparticles produced in a carbon arc

John Henry J. Scott and Sara A. Majetich*
Department of Physics, Carnegie Mellon University, Pittsburgh, Pennsylvania 15213
(Received 6 March 1995; revised manuscript received 11 July 1995)

The morphology and crystalline microstructure of carbon-encapsulated nanoparticles produced in a Huffman-Krätschmer fullerene reactor are studied systematically as a function of location within the reactor. X-ray powder diffraction and high-resolution transmission electron microscopy are used to characterize powder harvested from the reactor walls and the inner and outer cores of the cathode deposit. We observe increased graphitization and crystallinity, more faceting, and more gaps between the nanoparticle and the encapsulating carbon cages in the cathode deposit when compared to the wall powder. We propose a growth model based on gas-phase nucleation to explain these observations, linking carbon arc nanoparticle synthesis to existing work on gas aggregation cluster sources.

I. INTRODUCTION

Renewed interest in carbon arcs and arc products has arisen since the discovery of the Huffman-Krätschmer carbon arc process[1] for the production of fullerenes.[2] The availability of macroscopic quantities of fullerene-containing powder made possible by this technique quickly led to the discovery of other products of this process such as endohedral fullerenes,[3] carbon nanotubes,[4] larger graphitic carbon cages or "onions,"[5] and carbon-coated nanoparticles.[6–8] This last species, nanoparticles of metal or metal carbide wrapped in concentric layers of encapsulating graphitic carbon, has been studied recently by several groups.[9–20] A rich variety of materials have been found to encapsulate in the arc, including most of the rare earths and many transition metals. Exploitation of this technique for the production of ultrafine magnetic particles has been the chief interest of our group.[8,14] Our previous results have shown that encapsulated nanoparticles of ferromagnetic materials are predominantly monodomain and manifest the full range of fine-particle magnetic phenomena, including superparamagnetism and hysteresis below a blocking temperature. Interesting magnetic behavior and the oxidation resistance of the carbon coating have led to the consideration of these particles for application in areas such as magnetic data storage, magnetic toner for xerography, ferrofluids, and as contrast agents in magnetic resonance imaging. The potential of a one-step production process from simple feedstocks is also appealing.

Among the chief barriers to the immediate use of these particles in the proposed applications are broad size distributions, phase inconsistency, poor yields, and particle separation difficulties. Better knowledge of the growth mechanisms responsible for the formation of such particles during the arc process would help to surmount each of these obstacles. The main objective of this work has been to elucidate these growth pathways. Particle structure and morphology are both directly affected by the growth mechanism, and provide valuable information about the formation process. Our data systematically correlate location within the carbon arc reactor with these variables. Beyond cataloging encapsulation and characterizing the nanoparticle morphology for different materials, our experiments were designed explicitly to differentiate between competing carbon arc nanoparticle growth models. While our model assumes gas-phase growth, similar to the mechanisms responsible for inert gas aggregation cluster growth, all other models of carbon arc nanoparticle formation either propose cluster growth on the cathode surface or fail to address the issue.

In this work we describe a nanoparticle synthesis technique using a modified Huffman-Krätschmer carbon arc process and metal-carbon composite anodes. We describe in detail the characterization of the arc products by x-ray powder diffraction (XRD) and transmission electron microscopy (TEM). No attempt is made to characterize the growing particles in the arc itself. We also discuss changes in the morphology and structure of these arc products as the materials, abundance, He pressure, and location within the reactor are varied. These changes provide valuable clues about the formation environment of encapsulated nanocrystals produced in the arc and we propose a growth model based on these observations.

II. EXPERIMENTAL PROCEDURE

We used a variation of the Huffman-Krätschmer carbon arc process[1] to produce the nanoparticles described in this work. Graphite rods 6.35 mm in diameter were drilled down the center (3.18 mm diameter bore) and packed with metal or metal oxide powder, graphite powder, and graphite cement. The rods were then baked in air at 300 °C for at least 6 h to drive off moisture and cure the graphite cement. The rods, 20 cm in length, were consumed as the top electrode (anode) in our reactor. A water-cooled graphite cylinder was used as the bottom electrode (cathode). The arc was maintained by a 100 A current delivered at 30 V dc, while helium buffer gas was flowing through the reactor. Each rod took approximately 5 min to consume. While several groups have examined fullerene yields as a function of He pressure,[15] its effects on nanoparticle yield and morphology have received less attention. Over the course of several runs, the He pressure was varied from 75 to 925 Torr, and we found no discernible effects on nanoparticle morphology. The samples described in the remainder of this work were prepared in a He atmosphere at 125 Torr.

0163-1829/95/52(17)/12564(8)/$06.00

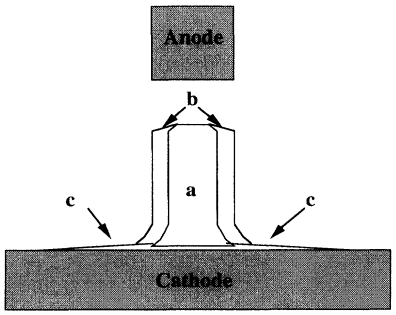

FIG. 1. Schematic of a typical cathode deposit, showing the inner core a, the outer core b, the pancake c, and the cathode itself.

The resulting arc products consisted of a fine powder coating the reactor walls and electrode supports, and a harder, pencil-like cathode deposit sitting atop a thin, flat, carbonaceous pancake covering the bottom electrode block (Fig. 1). The cathode deposit and pancake were removed from the reactor and the wall powder was collected with a brush. Samples were taken from each of the various arc products and each was ground with mortar and pestle into a uniform powder. These powders were not washed or magnetically separated.

Initial structural characterization by XRD was performed on a Rigaku diffractometer using a copper target. A post-sample graphite monochromator filtered out $K\beta$ but did not separate $K\alpha_1$ from $K\alpha_2$. Typical runs were at 35 kV, 20 mA, from 3° to 75° (2θ) in 0.05° steps. Each angle was integrated for 3 to 5 s. A sample holder made from single-crystal silicon wafers was used. No attempt was made to preserve random orientation in the sample, so line intensities may vary from those appearing in the powder diffraction file database.[21] To estimate the mass fraction sensitivity of our instrument, diffractograms of 2.8 wt % polycrystalline aluminum dispersed in powder generated from pure graphite rods were used. No aluminum peaks appeared in patterns taken with the intensity and integration time given above, indicating that 3 wt % is an *approximate* lower limit for dopant concentrations present in the powder yet undetectable by XRD. Higher fractions of nanophase material could go undetected because the size and reduced crystallinity of nanoparticles reduces the intensity of their Bragg peaks.

TEM was performed on all samples to determine particle size distributions and powder morphology. When possible, electron microdiffraction patterns were obtained to supplement XRD structural characterizations, and energy-dispersive x-ray spectroscopy (EDS) was done to determine the chemical composition of samples. TEM samples were prepared by grinding the raw powder with a mortar and pestle, dispersing a few milligrams in methanol, and sonicating for one half hour. The resulting suspension was pipetted onto a copper or nylon TEM grid coated with an amorphous carbon film and allowed to air dry. Conventional transmission electron micrographs were taken with a JEOL 120CX TEMSCAN microscope operated at 120 kV. High-resolution micrographs were obtained with a JEOL 4000 EX operated at 400 kV. The sample preparation did not significantly alter the size distribution of the particles, because the distribution observed under TEM did not change with sonication time or grinding time.

Electron diffraction and XRD are sensitive to different fractions of the raw powder. The powder contains both nanocrystals and larger chunks of material. While TEM is able to produce spot or ring diffraction patterns from a relatively small active area (diameter <1 μm), XRD averages over a larger area of the sample (>1 cm), so care must be taken when interpreting XRD patterns and comparing them to TEM spot patterns.

III. RESULTS AND DISCUSSION

The electric discharge between the electrodes creates a hot spot on the anode and cathode; typical anode temperatures exceed 3750 K.[22] Such high temperatures atomize material from the anode and create a plasma around the arc that contains species derived from the carbon, dopant material, and He buffer gas. This is not a high-field region since most of the 30 V potential difference between the electrodes occurs within a few electron mean free paths of the electrode surfaces in the anode and cathode fall regions.[23,24] XRD and TEM have never revealed starting material phases in the reactor products, supporting the idea that electrode materials are vaporized rather than ablated from the anode under our conditions. As the material in this region diffuses outward and is cooled by the He buffer gas, clusters begin to condense from the vapor.

Cluster size, crystallinity, structure, and stoichiometry depend on several interconnected factors including material chemistry, thermodynamics, kinetics, and reaction conditions such as arc current, voltage, and length. To separate and understand these various factors, dopant material, reaction conditions, and powder sampling location were varied. Our results here include characterizations of powders recovered from runs of rods packed with oxides of europium and holmium, and cobalt metal. Our previous work has included oxides of gadolinium, iron, and nickel, and the alloys samarium cobalt and manganese aluminum.[8,14,16,18] Collectively, other groups have looked at a wide variety of materials, including all but one of the rare earths, gold, palladium, and platinum. In the following sections, the effects of materials chemistry and location within the reactor are extracted from powder characterization.

A. Materials chemistry

Not all materials encapsulate readily in carbon cages. Some materials form nanoparticles embedded within a matrix of amorphous carbon rather than isolated nanocrystals encapsulated in graphitic shells. Other materials do not embed or encapsulate, showing a low affinity for being enclosed by carbon. Figure 2 shows conventional transmission electron micrographs of powder containing metallic cobalt and Eu_2O_3 nanocrystals. Electron microdiffraction was used to determine the structure of the europium oxide nanoparticles; no evidence was seen for europium carbide or EuO, the starting material used to produce the europium particles. The micrographs indicate that the cobalt nanocrystals are embedded within a continuous matrix of carbon, while the europium oxide nanocrystals are fixed to the outside of the carbon globules. Saito and co-workers,[25] looking only at

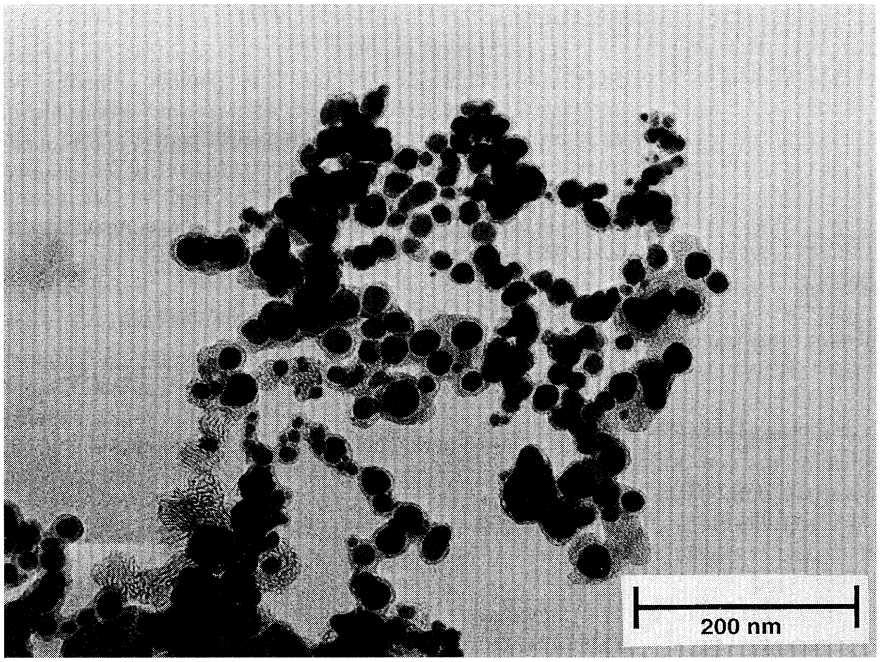

(a)

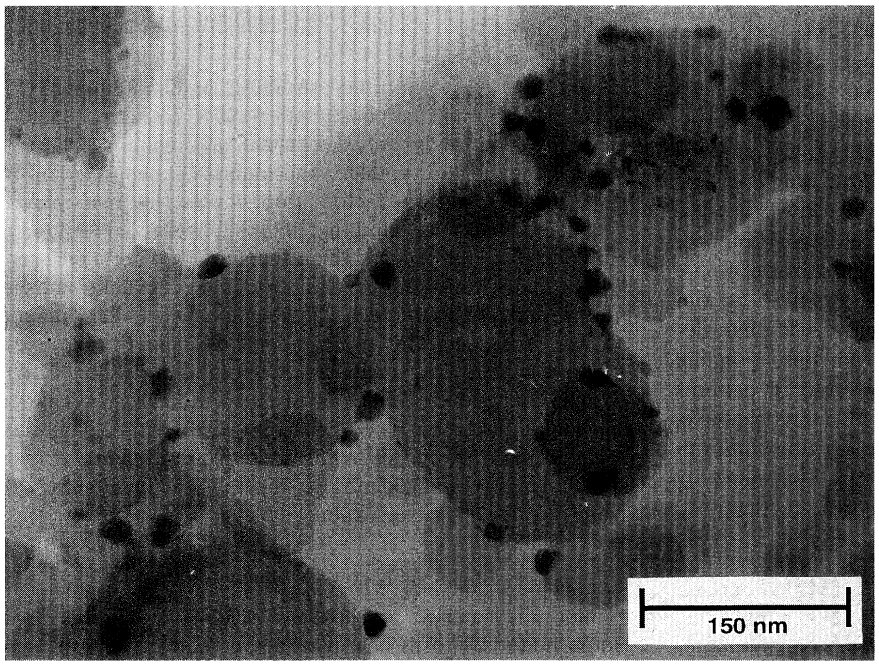

(b)

FIG. 2. (a) Transmission electron micrograph of wall soot cobalt nanocrystals embedded in a matrix of carbon. (b) Transmission electron micrograph of wall soot Eu_2O_3 nanocrystals adhering to the outsides of carbon globules. The europium oxide nanocrystals are not encapsulated in graphitic carbon.

cathode deposit morphology, have reported that most of the rare earths (Y, La, Ce, Pr, Nd, Gd, Tb, Dy, Ho, Er, and Lu) form encapsulated nanoparticles of the RC_2 phase (where R stands for one of the rare-earth elements), one (Tm) forms such nanoencapsulates only rarely, and one (Sc) forms carbide nanoparticles with the $R_{15}C_{19}$ structure. Under the same reaction conditions, three rare earths (Sm, Eu, and Yb) do not form encapsulated nanoparticles. Saito *et al.* noted a correlation between encapsulated nanocrystal formation and a relatively low elemental vapor pressure, compared to that for metals that do not encapsulate.

In addition to the interesting materials chemistry introduced into the system by the addition of rare earths and transition metals, the chemistry of carbon plays an important role in the formation of powder structures. Cobalt, for example, forms metallic nanocrystals in the face-centered cubic structure much more readily than it forms cobalt carbide nanocrystals. This is expected from the low solubility of carbon in cobalt as shown in the Co-C phase diagram.[26] Holmium, which is readily soluble in carbon, forms Ho_2C_3 and HoC_2 nanocrystals in the arc. Often clusters are formed far from equilibrium conditions allowing the production of

metastable phases in the powder, but the bulk phase diagrams are still useful in making qualitative predictions. The powders from the reactor walls share common morphological traits with carbon blacks and powders formed from other gas-phase processes, such as flame combustion.[27] In particular, fullerene blacks show aciniform structures (numerous fused spheres of nearly uniform size) and evidence of a post-aggregation growth process, where preformed spherules diffuse together and flocculate in the gas. In an earlier study of carbon blacks, the average spherule size was constant while the buffer gas was changed by four orders of magnitude. This was attributed to a model of growth followed by local depletion of the carbon feedstock to limit cluster size.[28]

B. Location within the reactor

Powders sampled from different locations within the reactor display variations in structure and morphology reflecting the differences in formation and annealing environments. Consumption of anode rods in the carbon arc produces several distinct structures in the reactor: a cathode deposit with a pencil-like center and a pancake base, and fine powder coating the reactor walls. This powder varies in color from black to gray and exhibits typical densities of 50 kg/m^3. The pancake consists of a smooth, thin, platelike scale covering the entire surface of the cathode. These carbon pancakes are thicker in the center (approximately 5 mm) than near the edge (less than 1 mm), and often exhibit a layered or laminar morphology, with laminae running parallel to the surface of the cathode. A cylindrical, pencil-like stem grows vertically from the center of the pancake, sometimes 30 or 40 mm tall; typical pencil diameters are 7–10 mm. This pencil structure consists of a soft, black inner core (approximately 2 mm in diameter) running its entire length, surrounded by a harder, gray outer core or shell. For arcs struck between pure carbon electrodes the morphology of this cylindrical deposit has been described in previous literature.[29,30] A 7 g composite anode typically produces 1–2 g of pencil deposit, 1–2 g of pancake, and 3–4 g of powder from the reactor walls. Generally, some material is lost to the vacuum system as CO, CO_2 or aerosols, and some material remains in the unburned anode stub.

XRD was used to identify the crystalline phases present in powder sampled from all of the structures mentioned above. Figure 3 shows diffraction patterns from holmium-containing powder collected from the reactor wall, the inner and outer cores of the cathode deposit, and the pancake. The holmium carbide example presented here is representative of those rare-earth carbides that readily form encapsulated nanocrystals. No evidence of the Ho_2O_3 starting material is seen in the patterns. The Ho-C phase diagram reveals two possible carbide phases, Ho_2C_3 and HoC_2, but only the dicarbide phase is observed by XRD. Electron diffraction spot patterns from TEM have confirmed the presence of the HoC_2 phase in the inner core and wall powder, and have shown that Ho_2C_3 nanocrystals are present in the wall powder at abundances below the expected sensitivity of XRD.[18] Peaks labeled "Si" are silicon peaks from the sample holder; peaks labeled "*G*" are identified as pure carbon peaks (graphite), and are observed in all patterns. The peak of 52.6° (labeled *C*) is also assigned to carbon because it appears in XRD of

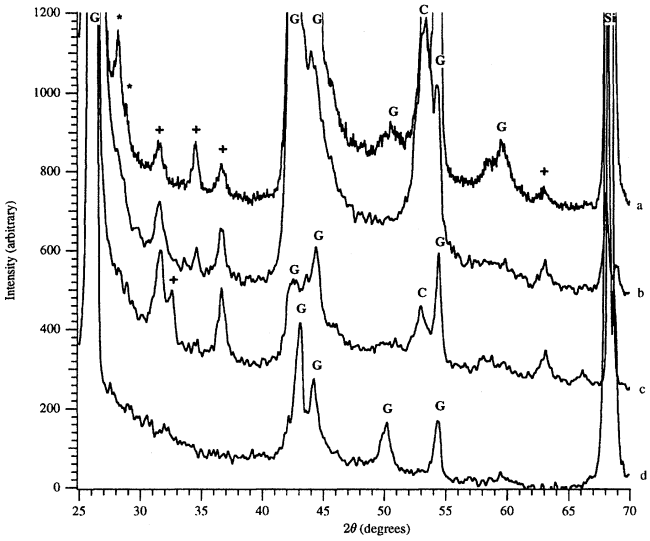

FIG. 3. XRD of holmium-containing powder sampled from (top to bottom) the inner core (curve *a*), the outer core (curve *b*), the cathode pancake material (curve *c*), and wall powder (curve *d*). *G* labels graphitic pure carbon peaks, Si is a silicon peak from the sample holder, asterisk labels HoC_2, and + are believed to be defect structures.

powder recovered from rods containing only carbon. Peaks at 28° and 29° in the inner core powder (labeled with an asterisk) are assigned to HoC_2, consistent with the rare-earth carbide phases found by other groups in the inner core.[25] The remaining peaks at 31°, 32°, 33.5°, 36°, 63°, and 66° (labeled with a plus) occur only for holmium-containing powders, but do not match any holmium, holmium-oxygen, or holmium-carbon phases in the powder diffraction database. These peaks are assigned to defect structures. High-resolution TEM of our samples reveals a large number of planar defects such as stacking faults. After annealing at 900 °C in an inert atmosphere, these peaks disappear. This temperature is high enough to increase diffusion rates and mobilities allowing the defects to heal, but it is much lower than the melting points of either carbon or the rare-earth carbides. Because the defected areas are very small, efforts to identify the metastable "phases" via electron microdiffraction have been unsuccessful. Complications such as these have made the characterization of bulk samples of nanocrystals less than straightforward. XRD has proven to be an invaluable tool for nanoparticle characterization, but XRD patterns should be interpreted with care, and in the context of results from other techniques.

A general trend revealed by XRD line shapes and intensities and confirmed by TEM is that cathode deposit powder is more graphitic than the wall powder, which appears to be more amorphous and disordered. This is attributed to the higher, sustained temperature of the cathode deposit compared to the material that condenses onto the (water-cooled) reactor walls. The higher temperature of the cathode allows the powder to anneal from an initially disordered state to a more crystalline state, as evidenced by the XRD.

Conventional TEM (CTEM) was used to characterize the microscopic morphology of material sampled from several locations within the reactor vessel. Every effort was made to

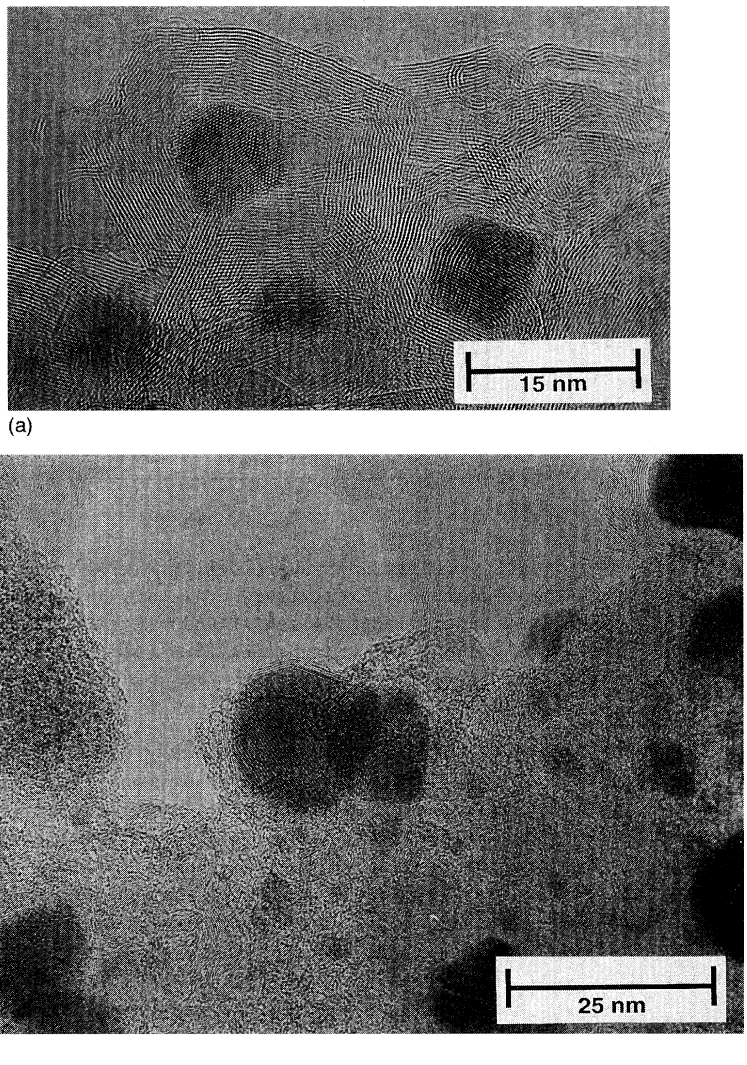

FIG. 4. (a) High-resolution transmission electron micrograph of Ho inner core powder showing increasing graphitization, increased faceting in the holmium carbide nanocrystals, and the presence of gaps between the nanocrystal and the surrounding carbon cage. (b) High-resolution TEM of a holmium carbide nanocrystal in wall powder. Graphitization and faceting are not as pronounced as in cathode deposit powder, and gaps are rarely seen.

choose typical, *representative* fields of view during microscopy and samples were prepared from thoroughly sonicated material to ensure maximum dispersion of particles and carbonaceous material. Unintentional bias introduced during microscopy due to overrepresenting interesting features or poorly prepared samples can obscure or distort morphological clues about the growth mechanism.

Figure 2(a) contains a typical micrograph of wall powder. While earlier growth models discussed particle formation on the surface of the cathode deposit,[10] observation of substantial numbers of nanoparticles in the wall powder implies a gas-phase growth pathway. Gas aggregation formation of nanoparticles is well known,[31–34] and we believe that a modified version of this process leads to the particles found at the reactor walls. A model that includes gas-phase growth is supported by the morphology of the pure carbon particles in the micrographs. The particles and aggregates of particles in these micrographs exhibit a reticulated, aciniform morphology very similar to that seen in carbon blacks produced in gas-phase processes, such as the incomplete combustion in air or the thermal decomposition of hydrocarbons. Carbon nanotubes were never seen in the powder recovered from our reactor walls, suggesting that these two species are formed by different mechanisms. Single-walled nanotubes catalyzed by transition metals have been observed in spiderweblike structures found by other groups throughout the reactor.[35] These likely have a gas-phase growth mechanism as well, but are much more sensitive to materials chemistry and other reactor conditions than the nanoparticles.

Micrographs such as these may also be used to determine particle size distributions for the metal or metal-carbide nanoparticles themselves. Measurement of equivalent spherical particle diameters from cobalt-containing powders yielded average particle sizes of 25 nm with very broad distributions (± 10 nm). (Particle size refers to the diameter of the inner core particle, without the carbon coating.) Generation and interpretation of such size distributions is complicated by the nonsphericity of some of the particles, and proper morphological characterization should include measures of higher-moment structure parameters such as anisometry.[36]

High-resolution transmission electron microscopy (HRTEM) was also performed on the powder to confirm and extend results obtained from conventional TEM. Figure 4

contains high-resolution micrographs of holmium-containing powder sampled from both the reactor wall and the inner core of the cathode deposit. In agreement with XRD results discussed earlier, the cathode deposit appears more crystalline than wall powder. This increased crystallinity is most evident in the pure carbon fraction of the powder. The graphitic shells surrounding nanoparticles are also more numerous in the cathode deposit samples (up to 40 layers per particle) than in wall powder. These results coupled with the XRD results suggest that graphitization is occurring at the cathode surface because of its elevated temperatures. Graphitization during the heat treatment of carbons is well known,[37,38] especially in the presence of catalyzing agents such as nanophase metals.[39]

A related morphological trend is the degree of faceting exhibited by the nanocrystals deposited in various reactor locations. Figure 4 shows increased faceting in inner core cathode deposit powder when compared to wall powder. If wall powder particles are quenched to low temperatures more quickly than cathode deposit material, the same annealing mechanism that increases the degree of crystallinity may be causing the increased faceting. Slower cooling rates may allow the nanocrystals to relax to a naturally faceted habit. The appearance of faceting in pure carbon systems such as thermal blacks and the similarity in facet angles and carbon shell morphology to that seen in carbon-coated nanoparticles suggests that such faceting is produced by a carbon-driven mechanism. Yet the role of transition-metal chemistry cannot be neglected. Transition metals are known to alter the graphitization of some carbons and catalyze the formation of carbon nanotubes. We observe far more facets in powders containing rare-earth carbide nanoparticles like HoC_2 (Fig. 4) than in powders containing transition-metal nanoparticles like metallic cobalt (Fig. 2). The interactions between the nanoparticle core and graphite coating that influence the degree of faceting observed in these particles are poorly understood at present.

Another striking feature of the nanoparticle shown in Fig. 4 is the presence of a gap between the nanocrystal and the surrounding carbon cages. Gaps such as these have been seen by a variety of groups,[7,9,11,13] mostly in systems containing rare-earth dicarbide nanoparticles. While it is difficult to conclude the details of the gap formation mechanism from data such as these, it is significant that gaps are seen frequently in cathode deposit powder, yet never in powder sampled from the wall.

C. Growth mechanism

Because of the intense interest in carbon nanotubes, carbon-coated nanoparticles were first discovered in the inner core of the cathode deposit, a structure rich in both of these species. Early attempts to explain the production of nanoparticles in the carbon arc were based on the morphology of particles found only in this region. Some of these attempts included simple bulk-phase thermodynamic arguments based on enthalpies of formation, but failed to produce an accurate predictor of nanoparticle formation and said nothing about the carbon coating or internal structure displayed by these particles. As the number of materials successfully encapsulated as nanoparticles increased, so did the base of evidence suggesting that materials chemistry plays an important role. Saito and co-workers[25] studied the entire lanthanide series (excluding Pm) and found a clear correlation between encapsulation and vapor pressure for rare-earth carbide nanoparticles. Low-vapor-pressure, nonvolatile metals produced encapsulated nanoparticles while the high-vapor-pressure, volatile metals (Sm, Eu, Tm, and Yb) failed to encapsulate. Based on these results, Saito *et al.* proposed a growth model in which nanoparticle formation occurs at the surface of the cathode, with a liquid metal-carbon alloy particle cooling while being bombarded by high-energy species from the vapor. As the particle temperature drops below the melting point of carbon, the outer graphite coating phase segregates and solidifies leaving a liquid core which eventually crystallizes to form a dicarbide nanoparticle. In this growth model the codeposition of metal and carbon atoms is indispensable to the formation process; relatively volatile rare earths do not encapsulate because they do not easily deposit onto the cathode from the vapor.

Our data are taken from a systematic study of the variation in morphology of powders sampled from various locations in the reactor. They suggest that previous growth models, based solely on observations from the inner core of the cathode deposit, should be modified and extended. In particular, the presence of nanoparticles in the wall powder indicates that the growth region in the reactor is not located on the cathode surface, but lies within or near the arc itself. Similarity in particle sizes and shapes provides strong evidence that all carbon-coated nanoparticles are created in a common growth region, and the abundance of particles in the wall powder precludes explanations based on ablation of preformed nanoparticles from the cathode by the arc.

Based on these points, we propose an alternative growth model. Carbon and anode dopant material is volatilized from the doped graphite rods because of the high current densities present in the arc. The resulting vapor is heated further as it passes near or through the arc plasma. The material is atomized, but it is not necessarily ionized, since the heat transfer from a low-pressure plasma to entrained particles is often small despite the extremely high temperatures. Studies in plasma torches indicate that particle dwell times of greater than 50 ms are necessary to vaporize 50 μm graphite particles in a 12 000 K steady-state argon plasma.[40] However, extensive searches for starting material phases (metal oxides) in the products of our carbon arc have never revealed them in any fraction, indicating that at least vaporization is occurring in our system.

As this vapor of carbon, metal, and helium diffuses to cooler regions, its temperature drops precipitously and it becomes supersaturated. Nucleation follows quickly, forming structurally fluid particles in a narrow size distribution. Continued adsorption of vapor onto existing particles and agglomeration of smaller particles into larger ones proceed depending on the steepness of the cooling curve and broaden the distribution significantly. From the point of nucleation onward, particle composition is determined by cluster-atom and cluster-ion affinities. These affinities manifest themselves in the bulk as partial vapor pressures and explain the correlation between rare-earth volatility and encapsulability. Melting-point differences between carbon and metal carbides lead to phase segregation and the formation of the carbon coating on the particle exterior. Recent experiments using

refractory materials have confirmed that, when this melting-point difference does not exist, the carbon does not segregate and carbon coatings do not form.[41] Further cooling takes place after the particle has condensed on the inside of the reactor or the cathode surface. Significant differences in these *postformation* environments result in different morphologies.

A growth model such as this highlights the similarities between the Huffman-Krätschmer process and more traditional gas aggregation cluster sources.[31–34] While the presence of novel structures such as nanotube and carbon-coated particles implies there is new physics in carbon arc growth, it is important to recognize its foundations in gas-phase cluster sources. Many groups have published observations of carbon arc products and microscopic evidence for novel structures, and a few have suggested growth mechanisms. We have combined the basics of gas aggregation with a carbon-coating formation mechanism in an alternative model which explains those materials which encapsulate and differences in morphology within the reactor.

IV. CONCLUSIONS

The Krätschmer-Huffman carbon arc method of producing fullerenes was used to produce carbon-coated nanoparticles from rare-earth and transition-metal precursors. We report observations from several experiments where powders were characterized by XRD and TEM, noting in particular the effects of materials chemistry, reaction conditions, and sample location within the reactor on powder structure and morphology. The correlations with sample location are to our knowledge the first in recent literature.

The similarity of the powder morphology to carbon black particles grown in the gas phase and the presence of significant numbers of encapsulated nanoparticles in the wall powder strongly imply that the carbon-coated nanoparticles collected from the reactor walls are formed in the gas phase. In agreement with other researchers, we observed that changes in the He gas pressure in the reactor during production have little effect on nanoparticle structure and morphology. Nanoparticles recovered from the cathode deposit, when compared to those harvested from the reactor walls, are found to be more crystalline, exhibit more faceting, and have more graphitic shells in their encapsulating coating. Gaps between the nanoparticle core and encapsulating shells are sometimes observed in cathode deposit powder, but are absent in particles collected from the reactor wall. These differences are attributed primarily to differences in the postformation environments of the particles in these locations; nanoparticles deposited on the cathode are "annealed" by the high temperatures created by the proximity of the arc.

ACKNOWLEDGMENTS

S.A.M. would like to thank the National Science Foundation for support through NYI Award No. DMR-9258308 and Grant No. ECD-8907068. The assistance of the CMU SURG program and the members of the CMU Buckyball Project have been invaluable. The authors would also like to thank N. T. Nuhfer and M. De Graef for technical assistance.

*Author to whom correspondence should be sent. Electronic address: sm70+@andrew.cmu.edu

[1] W. Krätschmer, L. D. Lamb, K. Fostiropoulos, and D. R. Huffman, Nature **347**, 354 (1990).
[2] H. W. Kroto *et al.*, Nature **318**, 162 (1985).
[3] Y. Chai *et al.*, J. Phys. Chem. **95**, 7564 (1991).
[4] S. Iijima, Nature **354**, 56 (1991).
[5] D. Ugarte, Nature **359**, 707 (1992).
[6] C. S. Yannoni *et al.*, Science **256**, 1191 (1992).
[7] R. S. Ruoff *et al.*, Science **259**, 346 (1993).
[8] S. A. Majetich *et al.*, Phys. Rev. B **48**, 16 845 (1993).
[9] M. Tomita, Y. Saito, and T. Hayashi, Jpn. J. Appl. Phys. **32**, L280 (1993).
[10] Y. Saito *et al.*, Chem. Phys. Lett. **204**, 277 (1993).
[11] Y. Saito *et al.*, Chem. Phys. Lett. **209**, 72 (1993).
[12] G. H. Taylor, J. D. Fitz Gerald, L. Pang, and M. A. Wilson, J. Cryst. Growth **135**, 157 (1994).
[13] S. Subramoney *et al.*, Carbon **32**, 507 (1994).
[14] M. E. McHenry *et al.*, Phys. Rev. B **49**, 11 358 (1994).
[15] S. A. Majetich *et al.*, in *Fullerenes: Physics, Chemistry, and New Directions VI, ECS Proceedings*, edited by K. M. Kadish and R. S. Ruoff (Electrochemical Society, Pennington, NJ, 1994), pp. 1448–1462.
[16] M. E. McHenry *et al.*, in *Fullerenes: Physics, Chemistry, and New Directions VI, ECS Proceedings* (Ref. 15), pp. 1463–1477.
[17] E. M. Brunsman *et al.*, J. Appl. Phys. **75**, 5882 (1994).
[18] B. Diggs *et al.*, J. Appl. Phys. **75**, 5879 (1994).
[19] S. Kirkpatrick, *et al.* (unpublished).
[20] S. A. Majetich, J. O. Artman, C. Tanaka, and M. E. McHenry, J. Appl. Phys. **76**, 6307 (1994).
[21] JCPDS-ICCD powder diffraction database.
[22] Y. Murooka and K. R. Hearne, J. Appl. Phys. **43**, 2656 (1972).
[23] A. M. Howatson, *An Introduction to Gas Discharges* (Pergamon, New York, 1965), p. 92.
[24] M. F. Hoyaux, *Arc Physics* (Springer-Verlag, New York, 1968), p. 184.
[25] Y. Saito *et al.*, J. Phys. Chem. **98**, 6696 (1994).
[26] *Binary Alloy Phase Diagrams*, 2nd ed., edited by T. B. Massalski (ASM International, Materials Park, OH, 1990), pp. 835–836.
[27] K. Kinoshita, *Carbon: Electrochemical and Physicochemical Properties* (Wiley, New York, 1988), p. 25.
[28] G. W. Smith, in *15th Biennial Conference on Carbon, 1981*, edited by W. C. Forsman (American Carbon Society, Philadelphia, 1981), p. 482.
[29] S. Seraphin, D. Zhou, and J. Jiao, Carbon **31**, 1212 (1993).
[30] S. Seraphin *et al.*, Chem. Phys. Lett. **217**, 191 (1994).
[31] C. G. Granqvist and R. A. Buhrman, J. Appl. Phys. **47**, 2200 (1976).
[32] H. Abe, W. Schulze, and B. Tesche, Chem. Phys. **47**, 95 (1980).
[33] S. Iwama and K. Hayakawa, Surf. Sci. **156**, 85 (1985).
[34] F. Frank *et al.*, Surf. Sci. **156**, 90 (1985).
[35] D. S. Bethune *et al.*, Nature **363**, 605 (1993).
[36] A. I. Medalia, J. Colloid Interface Sci. **24**, 393 (1967).
[37] D. B. Fischbach, in *Chemistry and Physics of Carbon*, edited by Philip L. Walker, Jr. (Dekker, New York, 1971), Vol. 7, p. 1.
[38] A. Pacault, in *Chemistry and Physics of Carbon* (Ref. 37), p. 107.
[39] H. Marsh and P. Warburton, J. Appl. Chem. **20**, 133 (1970).

[40] R. M. Young and E. Pfender, Plasma Chem. Plasma Process. **5**, 1 (1985).

[41] S. A. Majetich, J. H. J. Scott, E. M. Brunsman, and M. E. McHenry, in *Science and Technology of Fullerene Materials*, edited by P. Bernier, T. W. Ebbeson, D. S. Bethune, R. M. Metzger, L. Y. Chiang, and J. W. Mintmire, MRS Symposia Proceedings No. 359 (Materials Research Society, Pittsburgh, 1995), pp. 24–34.

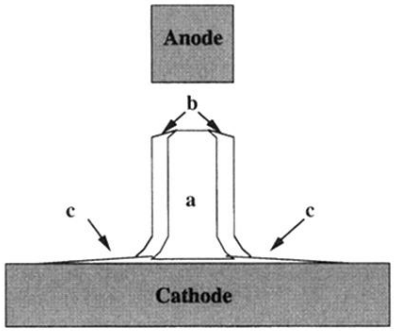

FIG. 1. Schematic of a typical cathode deposit, showing the inner core a, the outer core b, the pancake c, and the cathode itself.

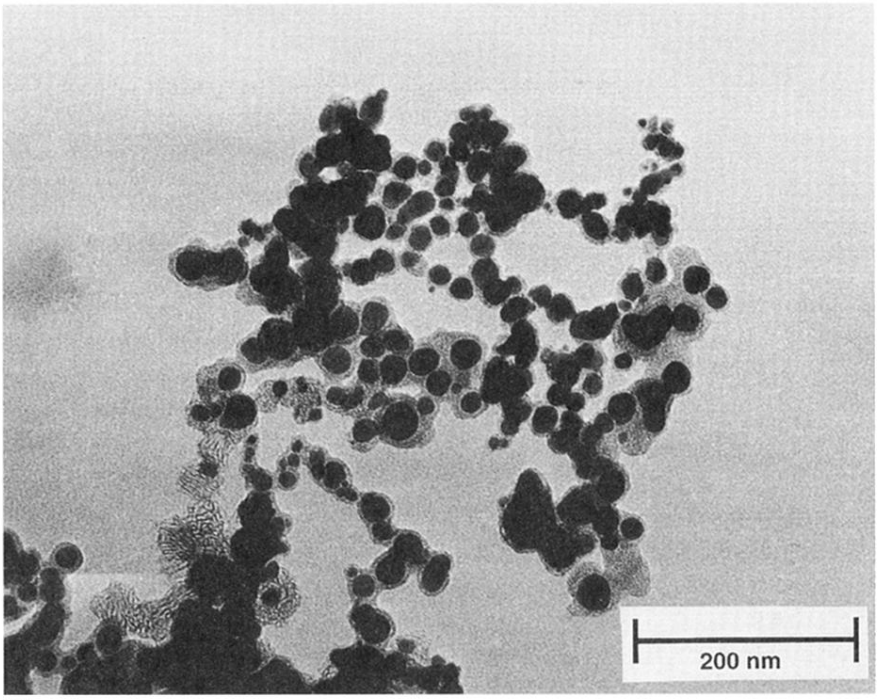

(a)

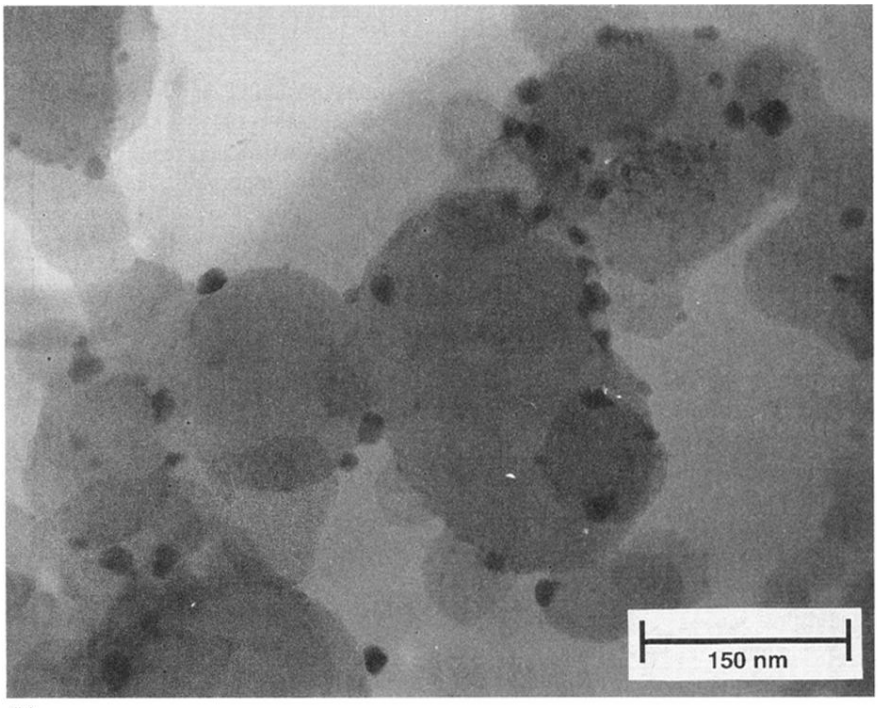

(b)

FIG. 2. (a) Transmission electron micrograph of wall soot cobalt nanocrystals embedded in a matrix of carbon. (b) Transmission electron micrograph of wall soot Eu_2O_3 nanocrystals adhering to the outsides of carbon globules. The europium oxide nanocrystals are not encapsulated in graphitic carbon.

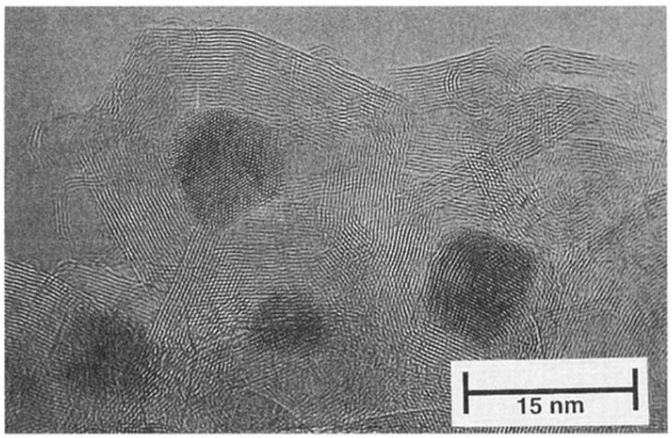

(a)

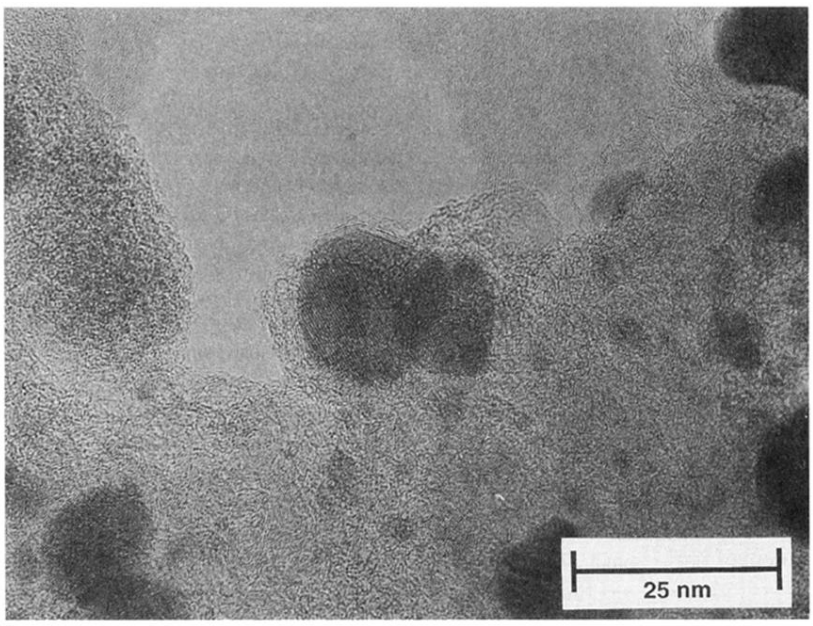

(b)

FIG. 4. (a) High-resolution transmission electron micrograph of Ho inner core powder showing increasing graphitization, increased faceting in the holmium carbide nanocrystals, and the presence of gaps between the nanocrystal and the surrounding carbon cage. (b) High-resolution TEM of a holmium carbide nanocrystal in wall powder. Graphitization and faceting are not as pronounced as in cathode deposit powder, and gaps are rarely seen.